Indian J Phys
https://doi.org/10.1007/s12648-021-02190-2

ORIGINAL PAPER

Logarithmic wave-mechanical effects in polycrystalline metals: theory and experiment

M Kraiev[1], K Domina[2], V Kraieva[3] and K G Zloshchastiev[4]*

[1]Yuzhnoye State Design Office, Dnipro 49008, Ukraine

[2]Z. I. Nekrasov Iron and Steel Institute of NAS of Ukraine, Dnipro 49107, Ukraine

[3]Department of Physics, Dnipro National University of Railway Transport, Dnipro 49010, Ukraine

[4]Institute of Systems Science, Durban University of Technology, Durban 4000, South Africa

Received: 19 April 2021 / Accepted: 12 August 2021

Abstract: Schrödinger-type wave equations with logarithmic nonlinearity occur in hydrodynamic models of Korteweg-type materials with capillarity and surface tension, which can undergo liquid–solid or liquid–gas phase transitions. One of the predictions of the theory is a periodic pattern of density inhomogeneities occurring in the form of either bubbles (topological phase), or cells (non-topological phase). Such inhomogeneities are described by solitonic solutions of a logarithmic wave equation, gaussons and kinks, in the vicinity of the liquid–solid phase transition. During the solidification process, these inhomogeneities become centers of nucleation, thus shaping the polycrystalline structure of the metal grains. The theory predicts a Gaussian profile of material density inside such a cell, which should manifest in a Gaussian-like profile of microhardness inside a grain. We report experimental evidence of large-scale periodicity in the structure of grains in the ferrite steel S235/A570, copper C-Cu/C14200, austenite in steel X10CrNiTi18-10/AISI 321, and aluminum–magnesium alloy 5083/5056; and also Gaussian-like profiles of microhardness inside an averaged grain in these materials.

Keywords: Wave mechanics; Polycrystalline metals; Logarithmic Korteweg material; Solidification; Microstructure

1. Introduction

Various crystalline structures occur in metals during the process of solidification. In pure metals, this is a simple crystal lattice, which can be of a cubic, body-centered cubic or face-centered cubic type. In real metals, a more complicated picture occurs, due to the presence of impurities, defects and other factors. Throughout the melt's bulk, multiple centers of nucleation occur, so that crystals begin to grow from those centers outward, until their boundaries reach each other. This is where interfaces develop between the borders of single-crystal domain grains. Finally, a polycrystalline structure occurs as a large-scale pattern of adjacent grains [1–3].

This leads to our first questions: How orderly is this pattern, and is the size and mass of each grain a completely random value? Aside from purely theoretical interest, such questions have immediate practical importance. The microhardness of grains, their size and density distributions, are very important properties of polycrystalline metals and alloys, because they strongly affect the macroscopic properties thereof, such as average hardness, plasticity, viscosity and mass [4].

These properties are formed when a grain nucleates from the molt during the solidification process. Using conventional statistical mechanics for such systems would result in a very cumbersome description, due to the complexity of its physical and chemical components. One could try to apply a "common wisdom" reasoning: because numerous impurities are randomly distributed in the molten bulk, and so are the associated nucleation centers, distances between those centers are expected to be random too. Consequently, one might anticipate that the distribution of grains' sizes would be uniform; or at least, would have some wide plateau-like distribution, so that no periodic large-scale pattern can form in the polycrystalline metals. But is this what actually happens?

*Corresponding author, E-mail: kostiantynz@dut.ac.za; kostya@u.nus.edu

Published online: 05 September 2021

It turns out that it is not. Numerous experimental data and metallographic analysis reveal that the distribution of grain sizes in cast metals is predominantly Gaussian, although it also depends on how the material is treated. Thus, during the collective recrystallization process, the distribution usually has a Gaussian form, with a shift toward larger sizes as temperature and soaking time on heating increase [5–7]. However, this distribution and relevant formulae have been established in those materials phenomenologically, while a proper theoretical explanation of the Gaussian behavior of grain size distributions is still pending.

This raises a further question: Is there an analytical way of explaining the matters raised above? For example, is it possible to find a set of effective collective degrees of freedom, in which the description of the materials in question can be substantially simplified, other than by using ab initio many-body statistical mechanics? Is it possible to find any universal laws and relations pertinent to the systems in question, or, at least, to a wide range thereof?

In this paper, we attempt to answer these questions, both on theoretical grounds, and by doing experimental studies of non-alloy structural steel S235/A570, copper C-Cu/C14200, stainless steel X10CrNiTi18-10/AISI 321, and aluminum–magnesium alloy 5083/5056. The paper is organized as follows. In Sect. 2, we give an overview of the logarithmic Korteweg-type model, both in its wave-mechanical and hydrodynamic representations, we also describe its phase structure. The predictions of the model pertinent to polycrystalline metallic materials are discussed in Sect. 3. The experimental setup and data are described in Sect. 4, where we used the Vickers hardness method for microhardness measurements of microstructure components. Discussion of results and conclusions are presented in Sect. 5.

2. The model

To address the problems mentioned in the Introduction, we use the wave-mechanical approach based on wave equations with logarithmic nonlinearity. This approach finds fruitful applications in the physics of condensed matter, to mention just a few of the literature landmarks [8–15]. The wide applicability and universality of logarithmic models can be explained by the fact that logarithmic nonlinearity appears in a leading-order approximation in the effective description of those strongly interacting many-body systems in which interaction energies predominate kinetic ones, and which allow a fluid-mechanical description, see Ref. [13] for details. Examples of such systems include not only low-temperature quantum Bose liquids, such as dense Bose–Einstein condensates [10, 12] or superfluid helium-4 [11, 14, 15]; but also Korteweg-type materials which can undergo liquid–solid or liquid–gas phase transitions [8, 16]. In these materials, capillarity and surface tension play a substantial role, which makes them useful for modeling various flows with non-negligible surface and interface effects [17, 18].

One of the theory's predictions is inhomogeneities of density, caused by the existence of multiple soliton and Gaussian-shaped solitary wave solutions for an underlying logarithmic wave equation in the vicinity of a liquid–solid phase transition. Each of these inhomogeneities can manifest themselves in the form of "bubbles" (density is smaller at the center of a domain than at its boundaries) or "cells" (density is larger at the center than at the boundaries). Recent studies of these phenomena were done for natural silicate materials in geophysics [16], such as magmas in volcanic conduits, where it is well-known that (approximately) periodical flows and structures occur [8].

2.1. Wave-mechanical representation

When molten metals cool to temperatures near their solidification point, the characteristic kinetic energies of their atoms become smaller than the interaction potentials between them. This can happen, not only at low temperatures, but also in high-density or effectively low-dimensional systems. Moreover, such materials behave more like fluids than solids or gases.

Therefore, following the line of reasoning of works [13, 16], we assume that, in a leading-order approximation: (1) one can apply a hydrodynamical description to such materials, by introducing a fluid function, which encodes the main properties of a flow, such as density and velocity, (2) the fluid function's dynamics is governed by a wave-mechanical equation, which somewhat resembles the Schrödinger equation, but with a nonlinear term, and (3) logarithmic nonlinearity occurs in this equation.

This equation can thus be written in the form

$$i\partial_t \Psi = \left[-\frac{\mathcal{D}}{2}\nabla^2 - b \ln\left(|\Psi|^2/\rho_0 \right) \right] \Psi, \tag{1}$$

where b, ρ_0 and $\mathcal{D}$ are real-valued parameters. Here, the fluid wave function $\Psi(\mathbf{x}, t)$ contains information about the fluid's macroscopic parameters, such as density and flow velocity; general discussion of such functions can be found in Ref. [19], for example. One can show that the nonlinear coupling b is a linear function of temperature, $b \sim T$, therefore, by setting $b = \text{const}$ from now on we assume that our fluid is in an isothermal state [13].

Equation (1) must be supplemented with the normalization condition

$$\int_V |\Psi|^2 \mathrm{d}V = \int_V \rho \, \mathrm{d}V = M, \tag{2}$$

where $\rho = \rho(\mathbf{x}, t)$ is fluid density, M and V are the total mass and volume of the fluid. This condition leads to analytical restrictions upon fluid functions: for the same set of boundary conditions, Eq. (1) allows multiple normalizable (eigen)solutions which correspond to excited states in the associated Hilbert space of the problem, for example L^2. In other words, a set of all fluid wave functions must form a Hilbert space, which can be interpreted as this fluid spontaneously "choosing" to be in one of these states (the ground state is still preferred, because it corresponds to the minimum of wave-mechanical energy).

Thus, the fluid function description is somewhat similar to the formalism of quantum mechanics, except that the fluid function is essentially macroscopic. It does not describe particles, but fluid parcels which are collective degrees of freedom, while their microscopic (molecular or atomic) structure is neglected. Nevertheless, one can still use the formal similarities between fluid functions and wave functions, as will be shown below.

2.2. Hydrodynamic representation

Let us write the fluid wave function in the Madelung form

$$\Psi = \sqrt{\rho} \exp(iS), \tag{3}$$

where $S = S(\mathbf{x}, t)$ is a phase, which is related to fluid velocity

$$\mathbf{u} = \mathcal{D} \nabla S, \tag{4}$$

under the simplifying assumption of irrotational flow.

Substituting Eq. (3) into Eq. (1), one obtains

$$\partial_t \rho + \nabla \cdot (\rho \mathbf{u}) = 0, \tag{5}$$

$$\partial_t \mathbf{u} + \mathbf{u} \cdot \nabla \mathbf{u} - \frac{1}{\rho} \nabla \cdot \mathbb{T} = 0, \tag{6}$$

with stress tensor $\mathbb{T}$ of the form

$$\mathbb{T} = -\frac{\mathcal{D}}{4\rho} \nabla \rho \otimes \nabla \rho - \tilde{p} \, \mathbb{I}, \tag{7}$$

where $\mathbb{I}$ is the identity matrix,

$$\tilde{p} = p(\rho) - \frac{1}{4} \mathcal{D} \nabla^2 \rho = -b\rho - \frac{1}{4} \mathcal{D} \nabla^2 \rho \tag{8}$$

is capillary pressure, and

$$p(\rho) = -b\rho \tag{9}$$

is a barotropic equation of state for the fluid pressure p. Tensor (7) belongs to the Korteweg class, which is used to model fluid mixtures with phase changes, capillarity effects and diffuse interfaces [17, 18].

Thus, Eq. (1) is a concise way of writing two hydrodynamic laws for mass and momentum conservation for a two-phase compressible inviscid fluid with internal capillarity whose flow is irrotational and isothermal. This makes it useful for studies, especially considering the large amount of analytical information about logarithmic wave equations which is already known.

2.3. Phase structure and solutions

It is known that Korteweg-type material can be in different phases, depending on the sign of nonlinear coupling [16]. On the other hand, this coupling is also related to temperature. Therefore, the sign of b corresponds to phases occurring at the material's temperature being either above or below a certain critical value.

Cellular phase. For a positive coupling, the field-theoretical potential density is given by

$$\mathcal{V}(|\Psi|^2) = -b|\Psi|^2 \left[\ln(|\Psi|^2/\rho_0) - 1 \right] + \mathcal{V}_0, \tag{10}$$

where $\mathcal{V}_0 = 0$. This potential has an upside-down Mexican hat shape. The local degenerate maxima of this potential are located at $|\Psi| = |\Psi_e| \equiv \sqrt{\rho_0}$.

In this case, a solitary-wave solution of Eq. (1) has the form of a Gaussian parcel

$$\Psi_g^{(+)}(\mathbf{x}, t) = \pm \sqrt{\rho_g^{(+)}(\mathbf{x})} \exp\left(-i\omega_g^{(+)} t\right), \tag{11}$$

$$\rho_g^{(+)}(\mathbf{x}) = \tilde{\rho} \exp\left[-\frac{(\mathbf{x} - \mathbf{x}_0)^2}{\ell^2} \right], \tag{12}$$

$$\omega_g^{(+)} = b\left[\bar{d} - \ln\left(\frac{\tilde{\rho}}{\rho_0} \right) \right], \tag{13}$$

where $\bar{d}$ is the number of spatial dimensions, and

$$\tilde{\rho} = M/\tilde{V}, \;\; \tilde{V} = \pi^{\bar{d}/2} \ell^{\bar{d}}, \;\; \ell = \sqrt{|\mathcal{D}/(2b)|} \tag{14}$$

are the density peak value, effective volume and Gaussian width, respectively.

The solution $\Psi_g^{(+)}$ corresponds to the state with the lowest frequency eigenvalue, $\omega^{(+)}$, which makes it analogous to the ground state in wave mechanics. It has been extensively studied since Rosen's work [20].

Thus, if nonlinear coupling is positive, then our material tends to fragment into clusters of density inhomogeneities with a Gaussian profile each, referred to here as cells. In the multi-solution picture, this results in a phase which is a composition of Gaussian-like cells. If this phase occurs in the melt of a metal, then during the solidification process

the central regions of these cells are likely to become nucleation centers; resulting in a polycrystalline structure.

Foam phase. If the nonlinear coupling is negative, then the potential (10) has a habitual Mexican-hat shape, assuming $\mathcal{V}_0 = -b\rho_0 = |b|\rho_0$. Its local maximum is located at $|\Psi| = 0$ and local degenerate minima are located at $|\Psi| = |\Psi_e|$. These minima correspond to the state with the lowest eigenvalue of frequency $\omega_g^{(-)} = 0$. This indicates the presence of multiple topological sectors in the model, as well as topologically nontrivial solitons which interpolate between these minima.

To the best of our knowledge, no topological solutions have been found in an analytical form, but their existence can be revealed by numerical studies. In $\bar{d}$-dimensional space, in Cartesian coordinates, this solution is searched in the form of a product of $\bar{d}$ 1D kink solitons

$$\Psi_s^{(-)}(\mathbf{x}, t) = \prod_{j=1}^{\bar{d}} \psi_j(x_j, t), \tag{15}$$

and each of these 1D solitons saturates the Bogomolny–Prasad–Sommerfield (BPS) bound and has a nonzero topological charge, $Q = \varrho_0^{-1/2}\left[\psi_j(x_j \to +\infty) - \psi(x_j \to -\infty)\right]$, $j = 1, \ldots, \bar{d}$, where $\varrho_0 = \rho_0^{1/\bar{d}}$. The plots of numerical solutions and corresponding densities can be found in Fig. 2 of Ref. [16].

Depending on the value of Q, all non-singular finite-energy solutions can be cast into four topological sectors [9]. For two of these sectors, the topological charge is not zero, ensuring the stability of the corresponding solitons. Thus, despite the kink solution being not the lowest frequency one, its stability against decay into a ground state Ψ_e is enhanced by a nonzero topological charge.

One can check that the mass density of the soliton, given by $\left|\Psi_s^{(-)}\right|^2$, grows from its center of mass outward, cf. Fig. 2 of Ref. [16]. Therefore, in three dimensions, the solution $\Psi_s^{(-)}$ can be viewed as describing a bubble with a characteristic size ℓ. In a single-solution setup, it would fill the entire space, but in a multi-soliton picture of real material, kinks and antikinks would alternate and match at distances of an order ℓ.

In other words, in this phase, our material forms foam-like structures, which facilitates the release of previously dissolved gas. Such a process can result either in boiling during the liquid–gas transition (if the temperature of the foam phase is larger than the temperature of the cellular phase), or in the formation of cavities in the bulk of the material, such as the pores and blowholes caused by decreased solubility and production of pertinent gases during solidification (if the temperature of the foam phase is smaller than the temperature of the cellular phase).

To summarize, depending on whether the temperature of the foam phase is larger or smaller than that of the cellular phase, the two-phase structure of our model can be used for describing both liquid–gas and liquid–solid transitions with formation of bubbles or cavities.

3. Theoretical predictions

When applied to liquid–solid phase transitions in polycrystalline metals, the logarithmic wave-mechanical model answers a number of the questions raised in the Introduction, such as is there any large-scale pattern in those metals' structure, and how one can derive or estimate hardness and density distributions. We shall deal with the application of our model to these problems, to more closely examine how it resolves them in Sects. 3.1 and 3.2, respectively.

3.1. Large-scale structure of metals

Let us assume that the melt can be described as a logarithmic Korteweg-type material, at least in a leading-order approximation. Then according to our model, its large-scale density profile has a pattern consisting of repeating solitary-wave (gaussons) or alternating (kinks–antikinks) solitonic solutions, depending on the phase our material is in. In other words, density inhomogeneities, which are not directly related to molecular bonding but are a collective nonlinear wave-mechanical phenomenon, emerge in a melt at a larger length scale.

In the case of metals undergoing a solidification process, those points, where the density profile reaches its extrema, are more likely to become the centers of grains' nucleation. Therefore, an average grain size is not random, instead its value must be close to the width ℓ given by Eq. (14).

3.2. Microhardness

Apart from the non-random distribution of grains at a large scale (about ten times the size of a grain, and above), our model predicts a Gaussian-like distribution of matter density inside a grain, i.e., from its center to the boundary. This has implications for the distribution of microhardness inside a grain, for the following reasons.

The non-uniform distribution of mechanical properties and density inside a grain is known to occur as a result of the following effects: segregation of chemical elements and repulsion of impurities from the center of a grain to its boundary during the crystallization process, the formation of stresses, as well as defect clusters of the crystal structure (dislocations), at the grain's boundary [1, 2, 21, 22]. These processes start to occur in the melt, alongside the formation

of crystals' seeds. Strength distribution depends on the stage the crystallization process is in, as well as on the quantity and size of seeds and liquid metal zones between them [3]. The crystals thus become spatial regions with larger hardness.

A qualitative correspondence exists between non-uniform distributions of strength and local density inside a grain. Variations of local density across a grain and the formation of regions of higher and lower density are caused by the accumulation of crystal grate defects, such as dislocations and vacancies. The higher probability of defects being located toward the grain's boundaries leads, on average, to lower values of density at the boundaries [23, 24].

The redistribution of density inside the melt region of a size comparable to the size of the future grain occurs during the melt's cooling and crystallization. Metals have a lower density in a liquid state than in a solid one, cf. steel: 6500–6800 versus 7700–8000 kg/m^3, copper: 8217 versus 8930 kg/m^3, and aluminum: 2382 versus 2700 kg/m^3.

As the melt cools, the growth of crystals from crystallization centers increases the volume of denser matter, until the boundaries of different grains touch each other. In the crystal which is thus forming, the redistribution of density occurs from its center to its boundary (with a minimum at the boundary), due to the abovementioned effects as a result of defects. This is a continuous process until the temperature reaches about half of the alloy's melting temperature. In a completely solidified grain, hardness and density both follow a normal distribution, but in an anti-correlated way: hardness has a maximum value at the grain's boundary, whereas density achieves its maximum in the center. The plastic deformation of a grain might increase the amplitude of this distribution, but it does not qualitatively change its main feature.

Therefore, our model predicts the periodic distribution of hardness across the specimen, with the average period being equal to the average size of a grain; and both of these values being equal to the characteristic length scale ℓ.

In the next section, we compare these predictions with experimental data.

4. Model-experiment comparison

To confront our model predictions with experiment, we study a number of the most common polycrystalline metallic materials: structural steel S235/A570, copper C-Cu/C14200, stainless steel X10CrNiTi18-10/AISI 321, and aluminum–magnesium alloy 5083/5056.

The microstructure of steel S235/A570 consists of the ferrite (light regions in Fig. 1a) and pearlite (dark regions in Fig. 1a phases; their ratio is about 75/25, respectively. Ferrite grains mainly have an equiaxial structure, with the exception of a few stringer grains of an elongated shape. They have no particular spatial orientation, and their size is about 20 μm. Sizes of pearlitic microconstituent grains for this steel vary between 5 and 45 μm.

The microstructure of the copper alloy specimen consists of approximately equiaxed grains of a size about 100 μm, see Fig. 1b. Similarly to the previous material, a few stringer grains of an elongated shape are present. Also, deformation twins can be found inside the grains.

The microstructure of the stainless steel specimen is austenitic and consists of polyhedral grains of a size of about 100 μm on average, Fig. 1c. As in the copper specimen, one can also encounter deformation twins in this steel.

Finally, the microstructure of the aluminum alloy specimen consists of approximately equiaxed grains of a size about 30 μm, see Fig. 1d. A small quantity of secondary ferric and silicon phases can be found both inside the grains and on their boundaries.

Based on this data and using Eq. (14), one can deduce a bound for the parameters of the models for each of the specimens. We obtain that $|\mathcal{D}/b| \approx 0.8 \times 10^{-9}$ m^2 for ferrite steel, $|\mathcal{D}/b| \approx 2 \times 10^{-8}$ m^2 for copper alloy and stainless steel, and $|\mathcal{D}/b| \approx 1.8 \times 10^{-9}$ m^2 for aluminum alloy.

Furthermore, microhardness measurements were performed for the abovementioned materials, using the Vickers hardness method. The load during the measurements was chosen according to the size of an indentation in a specimen. The test force was chosen to be either 0.025 or 0.05 N, depending on the grain's size, according to ISO 6507-1:2005(E) specifications. The points of the load's application were in the following areas of the grain: the grain's center, half-way to the grain's boundary, near the boundary, and on the boundary. Measurements were performed with a statistical dataset of 40–90 points per sample. The subsequent statistical analysis was performed at a confidence level of 95%, see Table 1. The profiles of microhardness measured across each specimen for the chosen materials are presented in Fig. 2.

Let us compare the experimental results with our theoretical predictions. Because hardness is related to the density of a material, theory predicts the occurrence of a periodic structure at length scales which are larger, by an order of magnitude, than the size of an average grain. The experimental data confirm this conjecture, see the left-hand side plots in Fig. 2. Statistical analysis confirms that the average size of the grains is not random: its distribution is far from being uniform, but always has a clear global

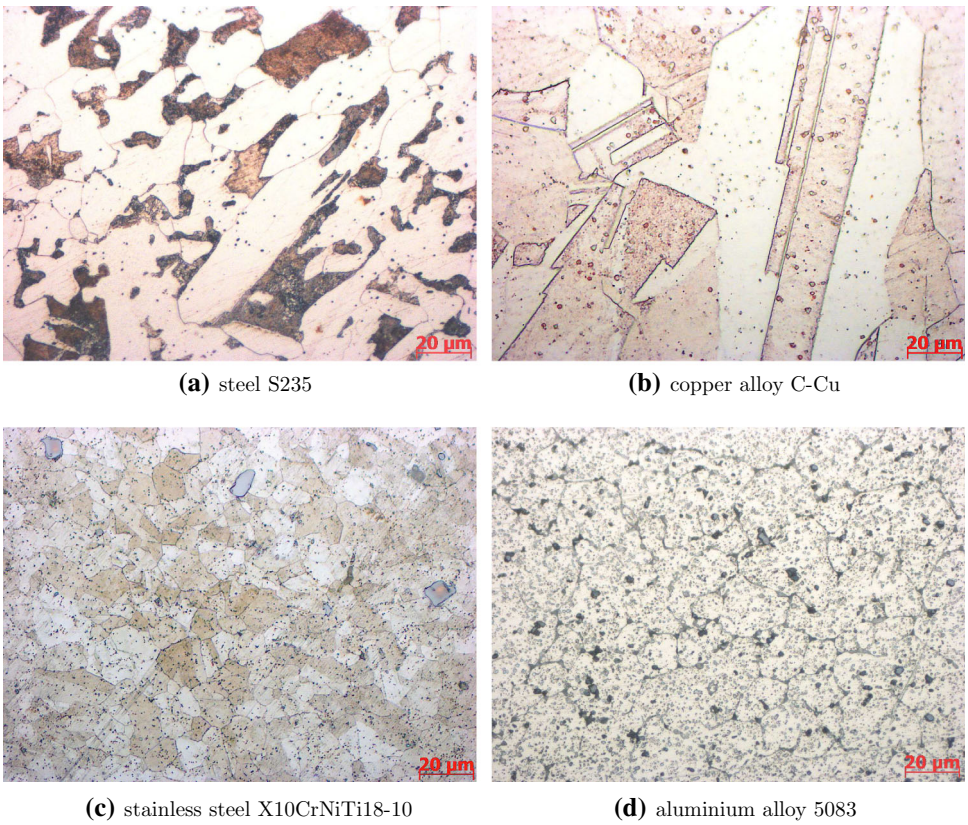

Fig. 1 Microstructure of the studied materials

(a) steel S235 **(b)** copper alloy C-Cu

(c) stainless steel X10CrNiTi18-10 **(d)** aluminium alloy 5083

Table 1 Microhardness distribution inside a grain

Alloy	Microhardness (HV)			
	At the center	Halfway to boundary	Near the boundary	At the boundary
Ferrite S235	77 ± 3	87 ± 3	94 ± 3	98 ± 4
Copper C-Cu	74 ± 3	78 ± 3	81 ± 3	96 ± 4
Austenite X10CrNiTi18-10	205 ± 5	224 ± 5	244 ± 6	269 ± 9
Aluminum 5083	79 ± 3	87 ± 2	92 ± 2	98 ± 3

maximum, regardless of the material, cf. the right-hand side plots in Fig. 2.

Furthermore, if the distribution of hardness inside each grain is anti-correlated with the distribution of density, the data confirm that the latter must have a Gaussian-like form, as predicted by the model. The measured average sizes of the grains thus provide an experimental bound for the Gaussian widths of the soliton-type solutions ℓ for each material studied.

5. Conclusions

In this paper, we considered the so-called logarithmic Korteweg-type materials, which are hydrodynamic models using wave equations with logarithmic nonlinearity. Their corresponding solutions have either trivial and non-trivial topology—when coupling is, respectively, positive or negative.

These models were applied to various materials, such as polycrystalline alloys, which undergo liquid–solid or liquid–gas phase transitions. Such materials have a two-phase structure, where each phase is labeled by a sign of the coupling of logarithmic nonlinearity and described by abovementioned solutions.

From a physical point of view, such solutions describe the density inhomogeneities, which can manifest themselves in the form of either bubbles (cavities) or cells in the vicinity of the liquid–gas (liquid–solid) phase transition. In materials undergoing a solidification process, these

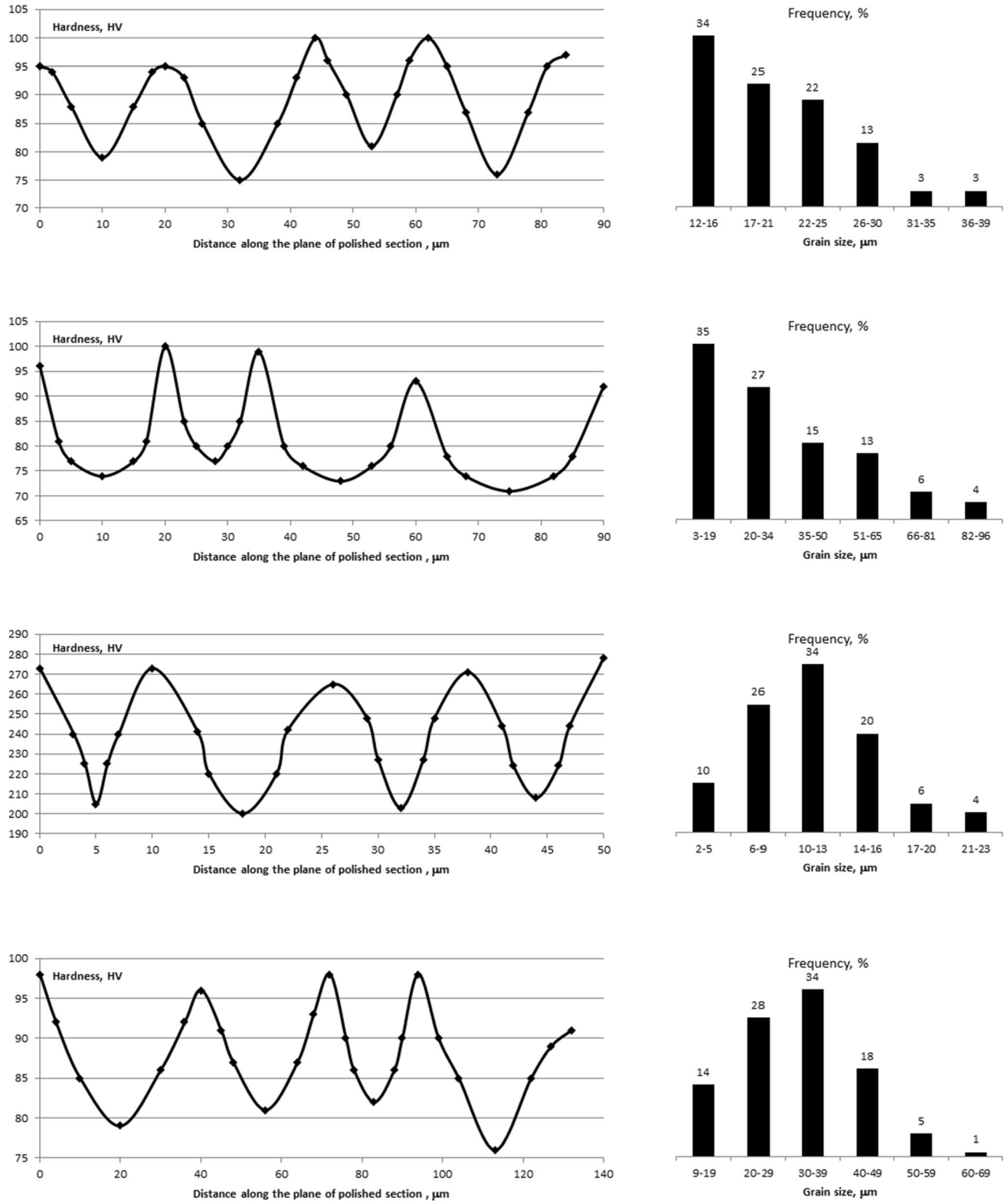

Fig. 2 Hardness profiles (left column) and grain size distributions (right column) in, from top to bottom: ferrite S235, copper alloy C-Cu, austenite X10CrNiTi18-10, and aluminum alloy 5083

inhomogeneities become centers of nucleation of grains occurring in the liquid phase in the vicinity of a melting point. One of the theory's predictions is a large-scale periodical Gaussian-like pattern, which occurs instead of expected randomness, if based on conventional statistical arguments. Due to additional processes and effects occurring during solidification, this periodicity can distorted, but not entirely destroyed.

The single-peaked (predominantly Gaussian) behavior of the distribution of grain sizes was established phenomenologically a long time ago [5, 6], but its statistical-mechanical theoretical explanation was hitherto unknown, to the best of our knowledge. In this paper, the occurrence of Gaussian-like repeating patterns is not only explained on hydrodynamic and statistical-mechanical grounds, but also used for describing density and hardness of polycrystalline metals. This illustrates the importance of taking into account properties of non-solid (liquid and gas) phases of a solidifying material when trying to model its solid phase's mechanical properties.

In previous works, natural silicate materials, such as magmas in volcanic conduits, were considered [8, 16], and the (approximately) periodical flows and structures were established. In this paper, we reported experimental studies of the structural (quasi)periodicity, microhardness, density and size of grains in structural steel S235/A570, copper C-Cu/C14200, stainless steel X10CrNiTi18-10/AISI 321, and aluminum–magnesium alloy 5083/5056.

To conclude, the wave-mechanical logarithmic model explains spatial variations in density and hardness of polycrystalline metals originating from their liquid phase during the solidification process. At a microstructural level, domains of spatial density variations form, which have Gaussian profiles of values, and the peaks of their distribution functions strongly affect the polycrystalline structure of the metal grains. The obtained results, along with their comparison with experiment, indicate an applicability of the model of a Korteweg type to a wide range of polycrystalline alloys. This allows us to provide analytical estimates for some of their mechanical characteristics, which are most important for applications.

Acknowledgements K.G.Z. is grateful to participants of the XXVI International Conference on Integrable Systems and Quantum Symmetries (ISQS-26) for stimulating discussions and remarks [25]. This research is supported by the Department of Higher Education and Training of South Africa and in part by the National Research Foundation of South Africa (Grants Nos. 95965, 132202 and 131604). Proofreading of the manuscript by P. Stannard is greatly appreciated.

Availability of data and materials The data may be available from the first author upon request.

Declarations

Conflict of interest The authors declare no conflict of interest

References

[1] V Salli *Structure Formation in Alloys* (New York: Springer) p 114 (1964)
[2] I I Novikov and V S Zolotorevskiy *Dendritnaya Likvatsiya v Splavakh (Dendritic Segregation in Alloys)* (USSR: Nauka) p 156 (1966) (in Russian)
[3] M C Flemings *Solidification Processing* (New York: McGraw-Hill) p 364 (1974)
[4] S P A Gill and C J Campbell *J. Mater. Res.* **34** 1645 (2019)
[5] S A Saltykov *Stereometricheskaya Metallografiya (Stereometric Metallography)* (USSR: Metallurgizdat) p 446 (1958) (in Russian)
[6] S S Gorelik *Rekristallizatsiya Metallov i Splavov (Recrystallization of Metals and Alloys)* (USSR: Metallurgy) p 568 (1978) (in Russian)
[7] E J Lezinskaya and T N Buriak *Probl. At. Sci. Technol. Phys. Radiat. Eff. Radiat. Mater. Sci.* **3** 66 (2004)
[8] S De Martino, M Falanga, C Godano and G Lauro *Europhys. Lett.* **63** 472 (2003)
[9] K G Zloshchastiev *Acta Phys. Polon.* **42** 261 (2011)
[10] A V Avdeenkov and K G Zloshchastiev *J. Phys. B At. Mol. Opt. Phys.* **44** 195303 (2011)
[11] K G Zloshchastiev *Eur. Phys. J. B* **85** 273 (2012)
[12] K G Zloshchastiev *Z. Naturforsch. A* **72** 677 (2017)
[13] K G Zloshchastiev *Z. Naturforsch. A* **73** 619 (2018)
[14] T C Scott and K G Zloshchastiev *Low Temp. Phys.* **45** 1231 (2019)
[15] K G Zloshchastiev *Int. J. Mod. Phys. B* **33** 1950184 (2013)
[16] K G Zloshchastiev *Europhys. Lett. (EPL)* **122** 39001 (2018)
[17] J E Dunn and J B Serrin *Arch. Rat. Mech. Anal.* **88** 95 (1985)
[18] D M Anderson, G B Mc Fadden and A A Wheeler *Annu. Rev. Fluid Mech.* **30** 139 (1998)
[19] Yu A Rylov *J. Math. Phys.* **40** 256 (1999)
[20] G Rosen *J. Math. Phys.* **9** 996 (1968)
[21] S F Kiseleva, N A Popova, N A Koneva and E V Kozlov *Lett. Mater.* **2** 84 (2012)
[22] N A Koneva, L I Trishkina, A N Zhdanov, O B Perevalova, N A Popova and E V Kozlov *Phys. Mesomech.* **9** 87 (2006)
[23] V N Gridnev, V G Gavrilyuk and Yu N Meshkov *Prochnost i Plastichnost Holodnodeformirovannoj Stali (Strength and Ductility of Cold-Deformed Steel)* (USSR: Naukova dumka) p 231 (1974) (in Russian)
[24] O A Kaybyshev and R Z Valiyev *Granitsy Zeren i Svoystva Metallov (Grain Boundaries and Metal Properties)* (USSR: Metallurgiya) p 216 (1987) (in Russian)
[25] M Kraiev, K Domina, V Kraieva and K G Zloshchastiev *J. Phys. Conf. Ser.* **1416** 012020 (2019)